Available online at www.sciencedirect.com
ScienceDirect
Earth and Planetary Science Letters 258 (2007) 44–60
EPSL
www.elsevier.com/locate/epsl

Plate tectonic trigger of changes in pCO_2 and climate in the Oxfordian (Late Jurassic): Carbon isotope and modeling evidence

Beat Louis-Schmid [a,*], Pauline Rais [a], Philippe Schaeffer [b], Stefano M. Bernasconi [a], Helmut Weissert [a]

[a] *Geological Institute, ETH Zurich, 8092 Zurich, Switzerland*
[b] *Laboratoire de Géochimie Bioorganique, CNRS-UMR 7509, Université Louis Pasteur, 67200 Strasbourg, France*

Received 14 August 2006; received in revised form 8 February 2007; accepted 8 March 2007
Available online 16 March 2007
Editor: M.L. Delaney

Abstract

The transition from the Middle to the Late Jurassic was characterized by significant changes in oceanography and climate and by changes in global carbon cycle as shown in the C-isotope record. A prominent mid-Oxfordian positive excursion in bulk carbonate carbon isotope values ($\delta^{13}C_{carb}$) with an amplitude of more than 1‰ has been documented from many sections in the Northern Tethys realm. In this study we present new bulk organic matter C-isotope data ($\delta^{13}C_{org}$) from northwestern Tethys that do not record the mid-Oxfordian positive excursion in carbonate carbon. On the contrary, $\delta^{13}C_{org}$ decreases during the interval of the most rapid increase in $\delta^{13}C_{carb}$. We demonstrate that this decrease is not due to a changing marine–terrestrial organic carbon partitioning but that the contrasting isotope trends record peculiar environmental and climate changes which occurred near the beginning of the Late Jurassic. Using a simple carbon cycle model we show that an increase in atmospheric pCO_2 starting at modern levels could be the cause of contrasting trends in $\delta^{13}C_{carb}$ and $\delta^{13}C_{org}$. We suggest that a reorganisation of ocean currents related to the opening and/or widening of the Tethys–Atlantic–Pacific seaway, and a massive spread of shallow-sea carbonate production led to higher pCO_2. Model simulations indicate that this increase in pCO_2 may have triggered changes in the biological carbon pump and in organic carbon burial that can explain the Middle Oxfordian C-isotope record.

Keywords: carbon isotopes; pCO_2; climate; carbon cycle; model simulation

1. Introduction

The Late Jurassic carbon isotope stratigraphy is marked by a positive carbon isotope excursion of ~3‰ which has been dated as Middle Oxfordian in age [1]. This excursion has been identified in marine and terrestrial carbon isotope records from the western and northern Tethys and the Atlantic [1–9]. $\delta^{13}C$ of marine carbonate ($\delta^{13}C_{carb}$) increased in several steps during the Early and the Middle Oxfordian, culminating in a distinct shift of 1‰ within few 10^5 yr at the end of the *plicatilis* ammonite zone. Peak $\delta^{13}C_{carb}$-values reach >3‰ at the beginning of the *transversarium* zone [2].

Positive excursions in $\delta^{13}C_{carb}$ are attributed to enhanced relative burial of organic carbon in sediments, leading to the progressive depletion of ^{12}C in the ocean carbon reservoir [10,11]. High organic carbon burial may be triggered by large-scale volcanic processes pumping excess CO_2 into the ocean–atmosphere reservoir [11,12].

* Corresponding author. Tel.: +41 44 632 8553; fax: +41 44 632 1075.
E-mail address: beat.louis@alumni.ethz.ch (B. Louis-Schmid).

0012-821X/$ - see front matter © 2007 Elsevier B.V. All rights reserved.
doi:10.1016/j.epsl.2007.03.014

This "classic" mechanism, used to explain the positive excursions in the Cretaceous (Valanginian, Aptian [13]), is not readily applicable to the Oxfordian [2]. Geologic evidence for sources of increased volcanic CO_2 fluxes, such as large igneous provinces, is lacking [14], possibly except of high seafloor spreading rates [15].

At the time of the most rapid increase in the $\delta^{13}C_{carb}$-record, the Oxfordian experienced a strong temperature increase in middle latitudes. Evidence from different proxies indicates that water temperatures may have increased by 5 °C, accompanied by a trend to arid conditions on continents in low and middle latitudes [16–22]. It has been proposed that this warming trend corresponds with the termination of an ice-age at the Callovian–Oxfordian boundary, caused by atmospheric pCO_2 levels below 500 ppm [17]. The suggestion of low pCO_2 is corroborated by proxy data indicating that Late Callovian pCO_2 was close to modern values [23]. It has also been suggested that the warming was related to changes in physical oceanography related to the opening of the Atlantic [16]. However, the process ultimately causing climate change remains unclear.

In this study, we present new organic carbon isotope data ($\delta^{13}C_{org}$) with an estimated resolution of 10 to 20 kyr covering the interval of climate change. We combine our data with simulations performed with a simple model of the long-term carbon cycle, and propose that changes in physical oceanography due to plate tectonic movements triggering substantive production and accumulation of marine carbonate led to an increase in atmospheric pCO_2 from about 380 to 600 ppm. This increase caused a response of the earth system that can explain the Middle Oxfordian C-isotope record and matches climate proxy data.

2. Material and methods

2.1. Studied section

The studied composite section, exposed near Serres (SE-France), was deposited in the Tethyan Subalpine Basin, a deep epeiric basin influenced by tectonics related to the opening of the Alpine Tethys and the Atlantic (Fig. 1). The section is composed of three parts from two localities, Trescléoux and Oze, some 50 km apart. It has a total length of 265 m and spans the Early Oxfordian ammonite zone *cordatum* (only the topmost subzone *cordatum*), and the Middle Oxfordian zones *plicatilis* (subzones *vertebrale* and *antecedens*) and *transversarium* (subzones *parandieri*, *luciaeformis*, *schilli* and *rotoides* (partly)), according to the standard sub-mediterranean ammonite zonation (Fig. 2). The section is divided in two facies types. The upper Argovien facies is carbonate-rich, ranging between 50 and 90 wt.% $CaCO_3$, and forms an alternation of marlstones and limestones. The lower Terres Noires facies deposited during the *cordatum–antecedens* subzones consists of dark marlstones with carbonate contents commonly between 30 and 40 wt.%. Organic carbon contents

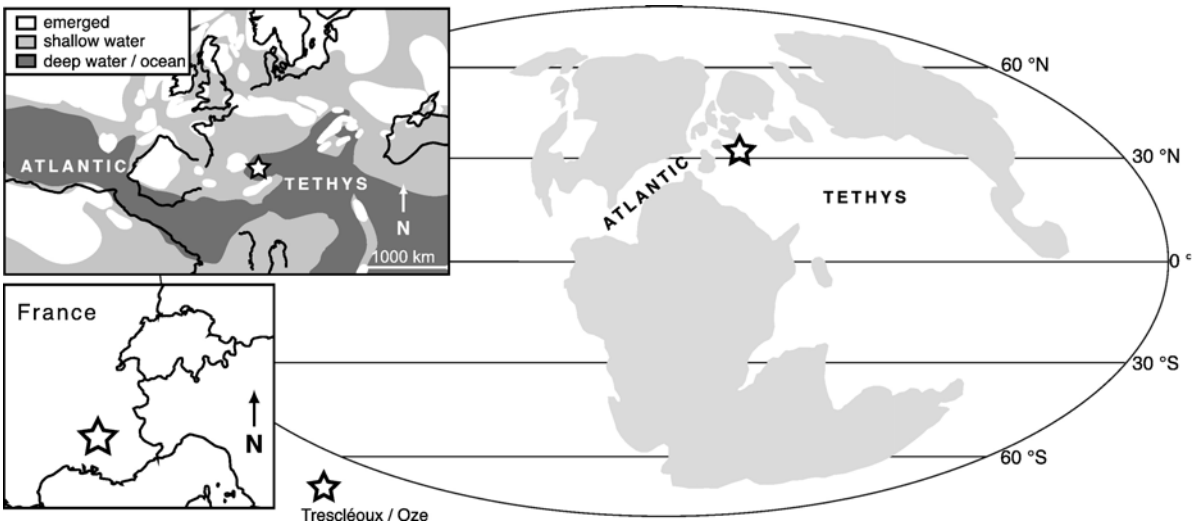

Fig. 1. Geographic and paleogeographic locations of the section studied, marked with a star. Right: Middle–Late Oxfordian paleogeography, land areas are shaded grey (after [75] in [68]). Upper left: close-up of western Tethys paleogeography during the Middle–Late Oxfordian, lines represent approximate positions of modern coastlines (after [76] and [77]). Lower left: location today of the section, lines represent state boundaries.

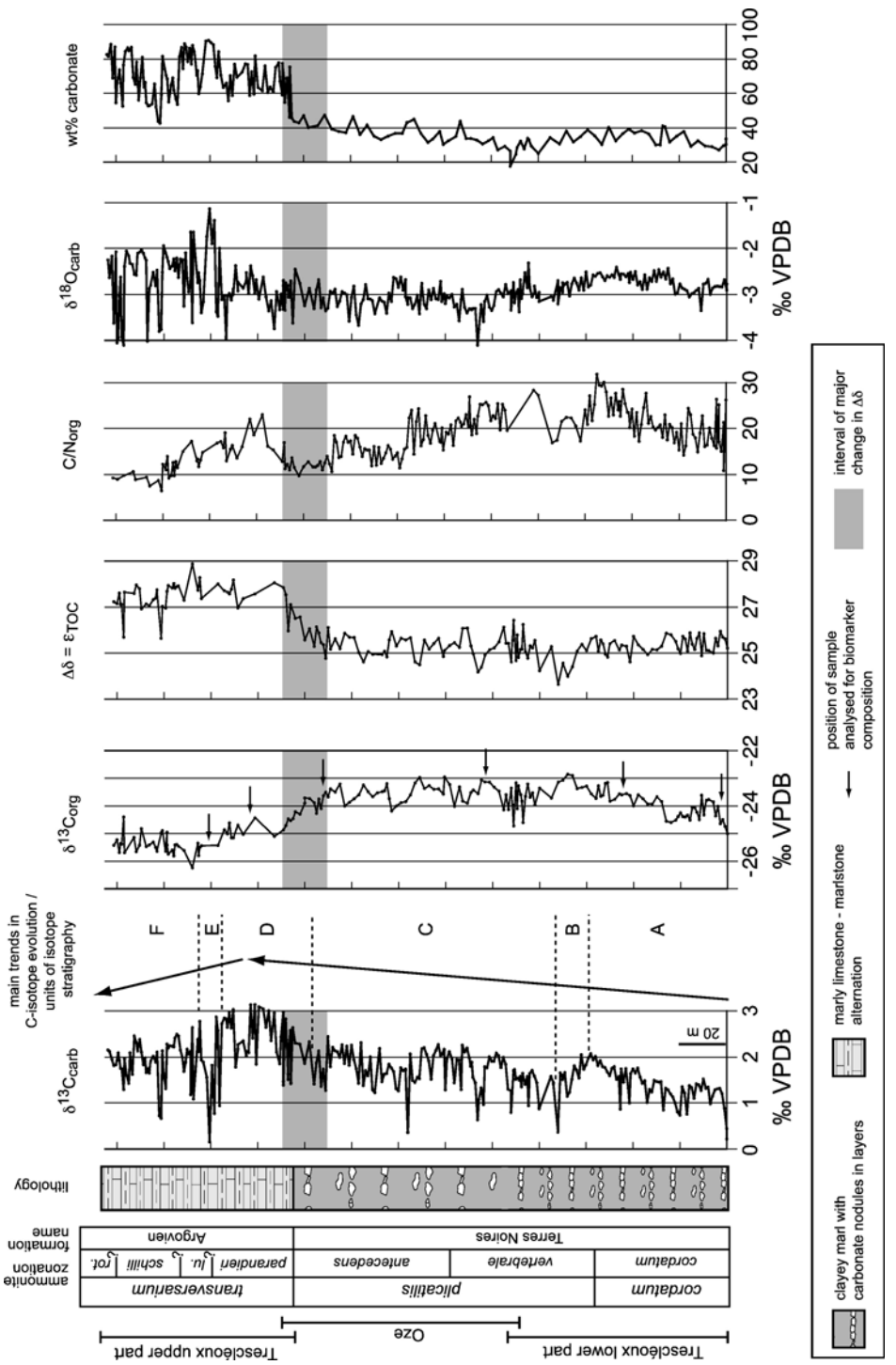

Fig. 2. Ammonite zonation, lithology, isotopic results, C/N-ratios and carbonate content of the section studied. Interval of major change in $\Delta\delta$ is shaded grey. Positions of samples analysed for biomarker composition are marked with arrows in the $\delta^{13}C_{org}$-column. Section log, $\delta^{13}C_{carb}$, $\delta^{18}O_{carb}$ and carbonate content from [2].

average 1% [24]. Organic matter is a mixture of mainly marine and sparse terrestrial material based on biomarker evidence (see Section 3.2.). Detrital minerals include clays and quartz, carbonate includes micrite, coccoliths, and foraminifera; macrofossils are rare and consist mainly of ammonites and belemnites. The marlstones are bedded at decimeter- to meter-scale. The carbonate carbon and oxygen isotope data in Fig. 2 are from [2].

2.2. Methods

Samples were drilled with a diamond-coated micro-drill bit. Secondary materials were carefully avoided while drilling. The powder was decarbonated in 1 N hydrochloric acid twice for 24 h, and homogenized after washing and drying. Organic matter carbon isotope compositions and carbon and nitrogen abundance were measured on a VG Optima mass spectrometer connected in continuous flow to a Carlo Erba Elemental Analyzer. Average precision of analyses, based on repeated measurements of the laboratory-internal standard atropina calibrated to NBS22, is ±0.16‰. All isotope values are reported in standard delta notation relative to the Vienna Pee Dee Belemnite (VPDB) (Fig. 2).

For biomarker analysis, cleaned samples were milled and at least 20 g each were extracted twice with dichloromethane (DCM)/methanol (MeOH) 1:1 v/v using an UP 200 s ultrasonic disrupter for 3 min. After removal of the elemental sulfur using activated copper, the extracts were concentrated under reduced pressure and evaporated under N_2. Following adsorption of the solvent extracts onto silica gel, the saturated hydrocarbon fractions and the polar fractions were separated by liquid column chromatography over silica gel, eluting with hexane and with DCM:MeOH 1:1 v/v, respectively.

The saturated hydrocarbon fractions were analysed by gas chromatography (GC) using a HP 6890 gas chromatograph equipped with an on-column injector, FID detector and a HP-5 fused silica capillary column (30 m × 0.32 mm; 0.25-μm film thickness). In order to investigate the polycyclic hydrocarbons present in minute amounts, one sample was analysed by gas chromatography-mass spectrometry (GC-MS) using a Varian 3400 gas chromatograph coupled to a Finnigan MAT TSQ 700 mass spectrometer operating in the electron impact mode (70 eV). Chromatographic separations were performed on a HP5-MS column (30 m × 0.25 mm; 0.1-μm film thickness) using helium (32 cm/s at 40 °C) as carrier gas and a temperature program of 40 °C–100 °C (10 °C min^{-1}), 100 °C–300 °C (4 °C min^{-1}), followed by isothermal at 300 °C.

3. Results

3.1. Isotope analyses

The measured trends in the $\delta^{13}C_{org}$-record do not parallel those in the $\delta^{13}C_{carb}$-record during parts of the Middle Oxfordian (Fig. 2). The $\Delta\delta$-curve, calculated as $\delta^{13}C_{carb} - \delta^{13}C_{org}$, can be divided in (i) a lower part with stable values between 25 and 26‰, (ii) a middle part representing a strong shift to higher values (shaded grey in Fig. 2), and (iii) an upper part with stable values around 28‰. See Fig. 2 for all results of isotope analyses.

3.2. Organic geochemistry

The saturated hydrocarbons from six samples covering the lower (samples TR 2 and TR 44), middle (OZE 18, OZE 314) and upper part (TRE 16, TRE 34) of the section have been investigated by GC, and one of them (TRE 16) by GC-MS. Position of these samples on the lithological column is shown in Fig. 2. The C_{16}^{+} hydrocarbons of all samples are dominated by straight-chain alkanes showing a monomodal distribution centered around the lower molecular weight homologues in the C_{18}–C_{20} range. For four out of the six samples analysed, this distribution does not show any carbon number predominance, as evidenced by the values of the carbon preference indexes (CPI; [25]) which are of 1.

$$CPI_{24-32} = 1/2\left[\frac{C_{25}+C_{27}+C_{29}+C_{31}}{C_{26}+C_{28}+C_{30}+C_{32}} + \frac{C_{25}+C_{27}+C_{29}+C_{31}}{C_{24}+C_{26}+C_{28}+C_{30}}\right]$$

This is generally considered as a typical feature for thermally matured hydrocarbons having reached the oil window ("petroleum-type" signature). However, in the case of the two samples from the upper section (TRE 16, TRE 34), a very slight odd over even carbon number predominance (CPI of 1.2 and 1.3, respectively) can be noted, likely indicating the contribution of land plant waxes and hence, of terrigenous inputs to the organic matter. The high maturity of the organic matter is further confirmed by the exclusive occurrence of hopanes having the thermodynamically more stable 17α(H),21β(H) configuration, together with the extent of epimerization of the stereocenter at C_{22} which shows a 22S/22R ratio obtained at thermodynamical equilibrium [26]. In all samples, the C_{16}+ n-alkane distribution is ranging from C_{16} up to C_{40} hydrocarbons.

Although the significance of the pristane–phytane (Pr/Ph) ratio is controversially discussed (e.g. [27]), we

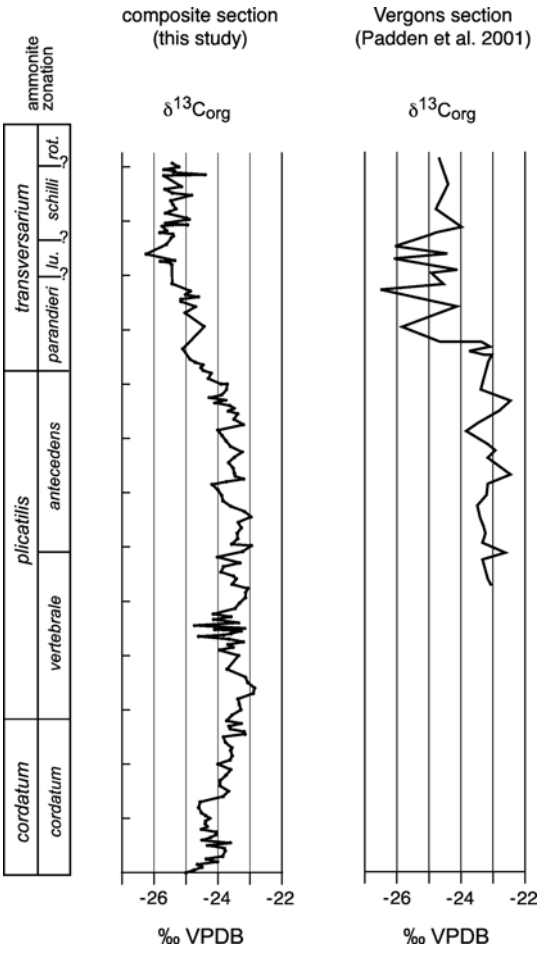

Fig. 3. Comparison between two organic matter C-isotope records. Left: our data; right: data from the Vergons section (SE-France), after [30].

use it as a first-order estimate of reducing versus oxidizing conditions at the time of deposition of the organic matter. When applicable with our samples, the Pr/Ph ratio shows values of about 1, which may be indicative of moderately reducing conditions. However, the use of such a ratio for palaeoenvironmental interpretations should be taken with caution in the case of thermally matured organic matter [28].

Polycyclic hydrocarbons are present in very low amounts, and occur essentially as pentacyclic hopane derivatives, which is an indication for the contribution of prokaryotic microorganisms, the latter being either primary producers (cyanobacteria), or heterotrophic bacteria. In contrast, tetracyclic hydrocarbons (i.e., steranes) from eukaryotic organisms (phyto- or zooplankton, terrestrial plants) were not detected.

These general biomarker distributions, as described above, are observed in the case of five out of the six samples investigated. Although following the same general characteristics regarding biomarker distributions, it can be noted that the n-alkane distribution from sample TRE 34 is enriched in higher molecular weight homologues in the C_{20}–C_{30} range, which may be attributed to additional biological inputs to the organic matter. The biological source(s) of these inputs remain however undetermined.

The C/N-record, if interpreted in terms of organic matter source, indicates that organic matter in the studied section is predominantly marine in the upper part of the section, and has a moderate terrestrial component in the lower part of the section [29]. The pattern of the C/N-record does not covary with $\delta^{13}C_{org}$ (Fig. 2), and the interval of the most intense change in $\Delta\delta$ (shaded grey in Fig. 2) is characterized by stable marine C/N-ratios.

3.3. Origin of the major change in $\Delta\delta$

To our knowledge, only few data have been published on the C-isotopic composition of organic matter in the Lower–Middle Oxfordian. These include data from a marine section in S-France [30] and data measured on fossil wood [3]. The S-France $\delta^{13}C_{org}$-curve is very similar to that presented here (Fig. 3). It is composed of three parts: a lower stable part with $\delta^{13}C_{org} \approx -23‰$, a middle decreasing part, and an upper stable part with $\delta^{13}C_{org} \approx -25.5‰$ [30]. The decreasing part is dated to be of middle *transversarium* zone age, i.e., it is in a stratigraphically higher position than the negative shift in the $\delta^{13}C_{org}$-record of our composite section. However, because of lacking biostratigraphical information, it was only assumed that the lower part of the section lies within the *transversarium* zone [1]. Based on lithological and $\delta^{13}C_{carb}$-correlation, it is likely that the lower part actually comprises parts of the *plicatilis* zone. The two records therefore carry a very similar C-isotope signal of the organic matter, indicating regional robustness of the record. Data from the Isle of Skye, Scotland, also show a very similar pattern (Elizabeth Nunn, personal communication). Therefore, and based on the results of organic geochemistry analyses, we assume that our data record original marine signals representing at least a broader area of the Tethys ocean.

Carbon isotope analyses of fossil wood showed that the $\delta^{13}C_{org}$-record of terrestrial organic matter parallels that of marine carbonate [3]. Our bulk organic matter data show an opposite trend (Fig. 2). Therefore, assuming that these are original marine signals, and based on the results presented in the sections above, we assume that the major change in $\Delta\delta$ (shaded grey in Fig. 2) is not due to an increasing contribution of terrestrial material, but due to a change in the isotopic fractionation between marine organic matter and

Table 1
Equations, formulas and constants employed in the model

Process/Constants	Mathematical expression
Change with time of the amount of inorganic carbon	$\mathrm{dDIC}/\mathrm{d}t = F_{\mathrm{volc}}(t) + F_{\mathrm{w,carb}}(t) + F_{\mathrm{w,org}}(t) + F_{\mathrm{meth}}(t) - F_{\mathrm{d,carb}}(t) - F_{\mathrm{d,org}}(t)$
Carbon flux from volcanic degassing	$F_{\mathrm{volc}}(t) = F_{\mathrm{volc\ (programmed)}}$
Carbon flux from carbonate weathering	$F_{\mathrm{w,carb}}(t) = F_{\mathrm{w,carb\ (programmed)}} \cdot f_{\mathrm{weathering}}$
Carbon flux from organic matter weathering	$F_{\mathrm{w,org}}(t) = F_{\mathrm{w,org\ (programmed)}} \cdot f_{\mathrm{weathering}}$
Carbon flux from methane hydrate dissociation	$F_{\mathrm{meth}}(t) = F_{\mathrm{meth\ (programmed)}}$
Carbon flux to carbonate deposition	$F_{\mathrm{d,carb}}(t) = F_{\mathrm{d,carb\ (programmed)}} \cdot f_{\mathrm{weathering}}$
Carbon flux to organic matter deposition	$F_{\mathrm{d,org}}(t) = F_{\mathrm{d,org\ (programmed)}} \cdot f_{\mathrm{nutrients}}$
Weathering factor	$f_{\mathrm{weathering}} = (p\mathrm{CO}_2(t)/p\mathrm{CO}_{2(\mathrm{steady\ state})})^{0.5}$
Atmospheric carbon dioxide concentration	$p\mathrm{CO}_2(t) = p\mathrm{CO}_{2(\mathrm{steady\ state})} \cdot (\mathrm{DIC}(t)/\mathrm{DIC}_{(\mathrm{steady\ state})})^{0.5} + p\mathrm{CO}_{2(\mathrm{programmed})}$
Nutrients factor	$f_{\mathrm{nutrients}} = [\mathrm{PO}_4^{3-}](t)/[\mathrm{PO}_4^{3-}]_{(\mathrm{steady\ state})}$
Phosphate concentration	$[\mathrm{PO}_4^{3-}](t) = [\mathrm{PO}_4^{3-}]_{(\mathrm{programmed})} \cdot f_{\mathrm{weathering}}$
Change with time of the isotopic composition of inorganic carbon	$\mathrm{d}/\mathrm{d}t(\delta_{\mathrm{DIC}}(t) \cdot \mathrm{DIC}(t)) = \delta_{\mathrm{volc}} \cdot F_{\mathrm{volc}}(t) + \delta_{\mathrm{w,carb}} \cdot F_{\mathrm{w,carb}}(t) + \delta_{\mathrm{w,org}} \cdot F_{\mathrm{w,org}}(t) + \delta_{\mathrm{meth}} \cdot F_{\mathrm{meth}}(t) - \delta_{\mathrm{d,carb}}(t) \cdot F_{\mathrm{d,carb}}(t) - \delta_{\mathrm{d,org}}(t) \cdot F_{\mathrm{d,org}}(t)$
Isotopic composition of volcanic carbon	$\delta_{\mathrm{volc}} \equiv -5‰$
Isotopic composition of weathered carbonate	$\delta_{\mathrm{w.carb}} \equiv 2.9‰$
Isotopic composition of weathered organic matter	$\delta_{\mathrm{w,org}} \equiv -22‰$
Isotopic composition of methane	$\delta_{\mathrm{meth}} \equiv -60‰$
Isotopic composition of deposited carbonate	$\delta_{\mathrm{d,carb}}(t) = \delta_{\mathrm{DIC}}(t) + ?_{\mathrm{d,carb}}$
Isotopic composition of sedimentary organic matter	$\delta_{\mathrm{d,org}}(t) = \delta_{\mathrm{d,carb}}(t) + ?_{\mathrm{d,org}}$
Fractionation between DIC and carbonate	$?_{\mathrm{d,carb}} \equiv 1.2‰$
Fractionation between carbonate and sedimentary organic matter	$?_{\mathrm{d,org}} \sim \varepsilon_{\mathrm{TOC}} = \varepsilon_{\mathrm{p}} + ?_{\mathrm{carb}} - ?_2$
Fractionation between CO_2 and primary biomass	$\varepsilon_{\mathrm{p}} = 25 - ((159.5 \cdot [\mathrm{PO}_4^{3-}] + 38.39)/[\mathrm{CO}_2])$
Fractionation between CO_2 and carbonate	$?_{\mathrm{carb}} = 11.98 - 0.12 \cdot T$
Isotopic difference between primary biomass and sedimentary organic matter	$?_2 \equiv 1.5‰$
Surface water concentration of CO_2	$[\mathrm{CO}_2] = \mathrm{kH} \leqslant p\mathrm{CO}_2$
Henry's constant	kH: calculated after Zeebe and Wolf-Gladrow [40]
Surface water temperature (°C)	$T = T_{(\mathrm{steady\ state})} + 10 \cdot \log(p\mathrm{CO}_2(t)/p\mathrm{CO}_{2(\mathrm{steady\ state})}) + T_{(\mathrm{programmed})}$

carbonate. This assumption is essential for the following discussion.

4. Carbon isotope fractionation between carbonate and organic matter

The difference between $\delta^{13}C_{carb}$ and $\delta^{13}C_{org}$ ($\Delta\delta$) may be used as an approximation of the average isotopic fractionation between total organic carbon (TOC) and sedimentary carbonate, defined as ε_{TOC} [31], if organic matter in the measured rocks is (predominantly) marine. ε_{TOC} mainly depends on (i) the physiology of primary producers, (ii) the concentration of CO_2 in surface water, and (iii) temperature [31–34]. The first two factors influence the fractionation between CO_2 in water and primary biomass produced by photosynthesizing phytoplankton, ε_P [32]. Temperature in turn controls largely the fractionation between CO_2 and total dissolved inorganic carbon (DIC) in water. As the isotopic composition of the DIC is the main factor determining the isotopic composition of marine carbonates, the isotopic relationship between dissolved CO_2 and carbonate, Δ_{carb}, also depends on temperature. Furthermore, as temperature influences the solubility of CO_2 in seawater, it influences ε_P (via the concentration of CO_2 in surface water). ε_{TOC} is then defined as the sum of ε_P and Δ_{carb} minus Δ_2, with Δ_2 being a correction factor for the isotopic difference between primary biomass and sedimentary organic matter [31]. Δ_2 accounts for secondary biological effects. However, also thermal maturation occurring during burial of the sediments may alter the C-isotopic composition of organic matter, although usually to a small degree [29,35]. Moreover, it is very likely that this effect was uniform throughout the investigated section and therefore did not alter the pattern of the $\delta^{13}C_{org}$-record. The relationships discussed in this section are summarized in Supplementary information 1, for calculation of the specific factors see Section 5 and Table 1.

The physiological factors contributing to the value of ε_P are difficult to assess and quantify individually [32]. However, the effects of these factors on ε_P can be summarized in a single value, which in the surface waters of the modern ocean is highly correlated to the concentration of phosphate, $[PO_4^{3-}]$ [36]. Assuming that this was also the case in the Late Jurassic, $[PO_4^{3-}]$ provides a means to estimate the impact of physiological factors on ε_{TOC}.

In order to evaluate possible individual and combined impacts of changes in pCO_2, $[PO_4^{3-}]$ and temperature on the Middle Oxfordian ε_{TOC}-record, we performed several simulations with a model of the long-term ($>10^5$ yr) carbon cycle.

5. Model description

5.1. Basic principle

The mass balance model of Wissler [37] (available as PDF-file at http://e-collection.ethbib.ethz.ch/show?type=diss&nr=14380) served as a starting point. This model calculates changes in the amounts of dissolved inorganic carbon (DIC), alkalinity, oxygen and calcium caused by imbalances in the respective fluxes into and out of a combined atmosphere–ocean reservoir. Additionally, as the carbon fluxes carry different C-isotope signatures, the model calculates $\delta^{13}C$ of the inorganic carbon reservoir. In this study, we only used the carbon part of this model. The change with time in the amount of DIC is described with a differential equation:

$$\begin{aligned} \mathrm{dDIC}/\mathrm{d}t = {} & F_{volc} + F_{w,carb} + F_{w,org} + F_{meth} \\ & - F_{d,carb} - F_{d,org} \end{aligned} \quad (1)$$

where F denotes carbon fluxes into or out of the reservoir that are due to volcanic outgassing (volc), weathering of carbonate rocks (w,carb), weathering of organic matter (w,org), methane hydrate dissociation (meth), deposition of carbonate in sediments (d,carb), and deposition of organic matter in sediments (d,org). The corresponding mass balance equation for changes with time in $\delta^{13}C$ of DIC is:

$$\begin{aligned} \mathrm{d}/\mathrm{d}t(\delta_{DIC}(t)\cdot \mathrm{DIC}(t)) = {} & \delta_{volc}\cdot F_{volc} \\ & + \delta_{w,carb}\cdot F_{w,carb} \\ & + \delta_{w,org}\cdot F_{w,org} \\ & + \delta_{meth}\cdot F_{meth} \\ & - \delta_{d,carb}(t)\cdot F_{d,carb-\delta_{d,org}}(t)\cdot F_{d,org} \end{aligned} \quad (2)$$

where $\delta_{DIC}(t)$ is the isotopic composition of the dissolved inorganic carbon, $\delta_{d,carb}(t)$ is defined as $\delta_{DIC}(t)+\Delta_{d,carb}$ with $\Delta_{d,carb}$=difference between isotopic composition of deposited carbonate and inorganic carbon, and $\delta_{d,org}(t)$ is defined as $\delta_{d,carb}(t)+\Delta_{d,org}$ with $\Delta_{d,org}$=difference between isotopic composition of deposited carbonate and organic matter.

5.2. Integrating time-dependent εTOC

For simplicity, Wissler [37] assumed $\Delta_{d,carb}$ and $\Delta_{d,org}$ to be constant. However, following the terminology of [30,31], $\Delta_{d,org}$ can be approximated by ε_{TOC}:

$$\begin{aligned} \Delta_{d,org} = {} & \delta^{13}C_{carb} - \delta^{13}C_{org} \approx \varepsilon_{TOC} \\ = {} & \varepsilon_p + \Delta_{carb} - \Delta_2 \end{aligned} \quad (3)$$

Thus, $\Delta_{d,org}$ is a variable depending on the factors outlined above. Possible values of Δ_2 are discussed in [31], we chose a constant value of 1.5‰. Δ_{carb} may be calculated using an empirical relationship [38]:

$$\Delta_{carb} = \delta^{13}C_{carb} - \delta^{13}C_{CO2} = 11.98 - 0.12 \cdot T \quad (4)$$

where T stands for temperature. Kump and Arthur [10] give the following formula to calculate ε_p:

$$\varepsilon_p = 25 - \left((159.5[PO_4^{3-}] + 38.39)/[CO_2]\right) \quad (5)$$

with $[CO_2]$ denoting the concentration of CO_2 in ocean surface water. Therefore, to introduce a time-dependent $\Delta_{d,org}$ into the model, we have to constrain $[CO_2]$, $[PO_4^{3-}]$ and temperature. $[CO_2]$ is related to pCO_2, the partial pressure of CO_2 in the atmosphere. Equilibrium exchange rates between these two reservoirs are described with Henry's constant [39], which allows to calculate $[CO_2]$ if pCO_2, temperature, salinity and pressure are known [40]. In our model, assuming a constant pressure of one atmosphere, we use a routine developed and described in detail by Zeebe and Wolf-Gladrow [40] to run this calculation.

5.3. Calculation of environmental conditions

On timescales of 10^4 to 10^5 yr, pCO_2 is mainly controlled by the amount of carbon dissolved in the oceans, assuming that the whole ocean is equilibrated with the atmosphere due to mixing, and that pH and alkalinity are basically constant. Hence, variations in pCO_2 may be estimated by relating them to variations in DIC [41]:

$$pCO_2(t)^* = pCO_{2(\text{ steadystate})} \cdot \left(DIC(t)/DIC_{(\text{ steadystate})}\right)^{0.5} \quad (6)$$

$pCO_2(t)^*$ then changes due to imbalances in the fluxes into and out of the reservoir, such as those caused by volcanism or methane hydrate dissociation. However, pCO_2 may also change due to ocean-internal mechanisms causing a different partitioning of CO_2 between deep and surface water, as pCO_2 is in equilibrium with the surface water concentration of CO_2 (e.g. [42,43]). This can be solved by adding a programmable additional amount of CO_2 to the value estimated by DIC content:

$$pCO_2(t) = pCO_2(t)^* + pCO_{2(\text{programmed})} \quad (7)$$

Thus, we are able to simulate rises in pCO_2 that do not stem from – but may trigger – a change in the ocean–atmosphere carbon reservoir size. We neglect changes to alkalinity of such a redistribution to satisfy Eq. (6) [41], and, for simplicity, we assume that these additional amounts of pCO_2 are net amounts after equilibration with the ocean [44].

Temperature is retrieved through the following relationship [41]:

$$T(t)^* = T_{(\text{ steadystate})} + 10 \cdot \log\left(pCO_2(t)/pCO_{2(\text{ steadystate})}\right) \quad (8)$$

Again, temperature calculated like this would only vary with changes in pCO_2. However, at the regional scale, temperature may also vary due to changes in ocean circulation. To be able to explore such forcings to regional temperature, we add a programmable temperature to Eq. (8):

$$T(t) = T(t)^* + T_{(\text{programmed})} \quad (9)$$

Finally, the evolution of $[PO_4^{3-}]$ with time is coupled to feedback mechanisms (see Section 5.4). With these routines, the model calculates time-dependent $\varepsilon_{TOC} \approx \Delta\delta = \Delta_{d,org}$, $\delta^{13}C_{carb}$ and $\delta^{13}C_{org}$.

5.4. Feedback mechanisms

The balance of the carbon cycle is maintained within certain boundaries by diverse feedback mechanisms [40,41,45–47]. To account for at least some of these, we introduced a feedback between pCO_2 and the weathering fluxes. It states that the weathering fluxes vary with the square root of $pCO_2(t)$ relative to pCO_2 (steady state) [41]. This includes all effects related to changes of pCO_2 that influence chemical weathering, i.e., temperature and precipitation, which are treated separately in more complex models (e.g. [48]). The weathering feedback mechanism is expressed mathematically as a time-dependent weathering factor:

$$f_{weathering} = \left(pCO_2(t)/pCO_{2(\text{ steadystate})}\right)^{0.5} \quad (10)$$

This weathering factor is then applied to the weathering fluxes, e.g., $F_{w,carb}$:

$$F_{w,carb}(t) = F_{w,carb(programmed)} \cdot f_{weathering} \quad (11)$$

Therefore, $F_{w,carb}$ is modulated by (optional) programmed changes superimposed by the feedback expressed in $f_{weathering}$. The same holds for all weathering fluxes in the model, in analogy to [41]. To maintain the pH of the ocean within reasonable boundaries, additional carbonate ions introduced to the ocean–atmosphere reservoir in the case of increased weathering of carbonates

need to be sequestered by producing carbonate [40] — a balance which is justified in the long-term carbon cycle as employed in our model. Mathematically, we solve this by coupling the deposition of carbonates, $F_{d,carb}$, to $f_{weathering}$.

Another feedback mechanism in our model incorporates the phosphate concentration in seawater, $[PO_4^{3-}]$. On time scales as employed in our model, phosphate is the ultimate limiting nutrient, and the rate of supply of phosphate to the ocean regulates total ocean productivity [49]. We therefore treat $[PO_4^{3-}]$ as a proxy for nutrient conditions of the ocean and state that the deposition of organic matter, $F_{d,org}$, will covary with relative changes in $[PO_4^{3-}]$ ($f_{nutrients}$). Hence, in our model, higher nutrient levels will favour the production and deposition of organic matter. This is a strong simplification in that productivity is not the only factor influencing preservation and burial of organic matter in sediments (others include availability of oxygen and sedimentation rates [50]). Additionally, to be able to account for such factors, the time-dependent behaviour of $F_{d,org}$ can be programmed. The time-dependent behaviour of $[PO_4^{3-}]$ can be programmed like the fluxes, but is also controlled by the weathering fluxes, such that an increase in weathering fluxes leads to an increase in $[PO_4^{3-}]$ — a relationship based on the fact that continental weathering is the most important source of phosphorus [51,52], but which is again a strong simplification as nutrient concentrations and productivity not only depend on weathering rates, but also, e.g., on oceanic mixing: for simplicity, we neglect changes in the magnitude of deep water nutrient remixing that arise from changes in the oceanic redox states [53,54]. The feedback between weathering and $[PO_4^{3-}]$ is mathematically implemented using $f_{weathering}$. Together with the $[PO_4^{3-}]$–$F_{d,org}$ feedback, it forms the nutrient feedback mechanism. All equations and mathematical expressions used in the model are listed in Table 1. We used Matlab® Simulink® to implement these equations and run the simulations.

5.5. Defining steady-state values

For steady-state DIC, we chose a value thought to represent a Mesozoic average situation [10]. For steady-state fluxes, we used figures of the present-day carbon cycle [55], some of them slightly adjusted to satisfy the steady-state terms in our model [37]. We further assume a salinity of 40‰ [56]. Temperature is initially set to 15 °C, representing an average value for the broader region of the section in the Early Oxfordian [18,57]. For $[PO_4^{3-}]$, we chose a steady-state value of 0.5 μmol kg^{-1}, an average value between oligotrophic and upwelling conditions [36]. With the above initial parameters, pCO_2 had to be set to 380 ppm in order to approximate the ε_{TOC}-value of the Middle Oxfordian prior to the interval of change (Fig. 2), a value that is in accordance to proxy data [23].

All chosen values for the steady-state situation are listed in Supplementary information 2. Using these figures, the model calculates steady-state values of

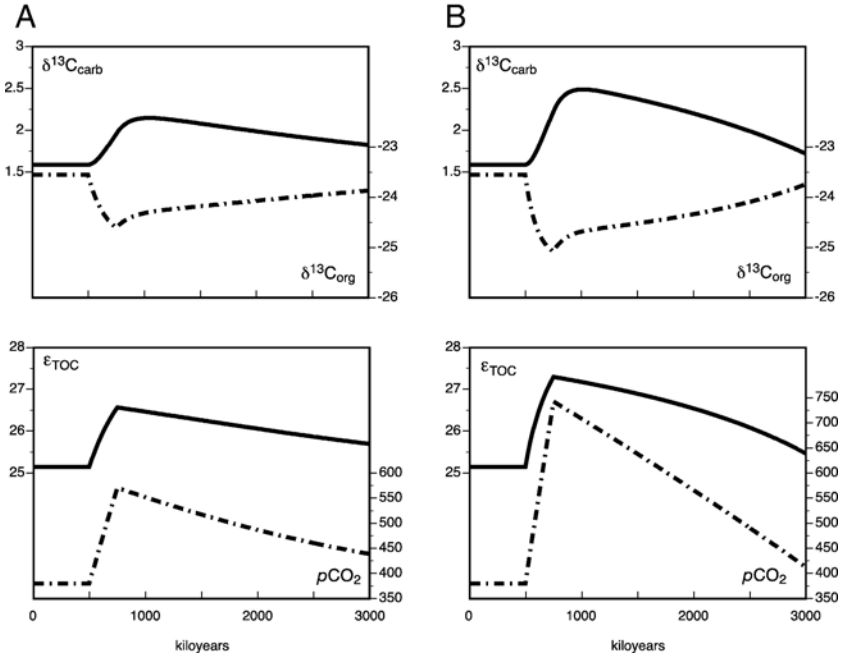

Fig. 4. Results of simulation I. Applied forcing: pCO_2 increase from 380 to 580 ppm from timestep 500 to timestep 750.

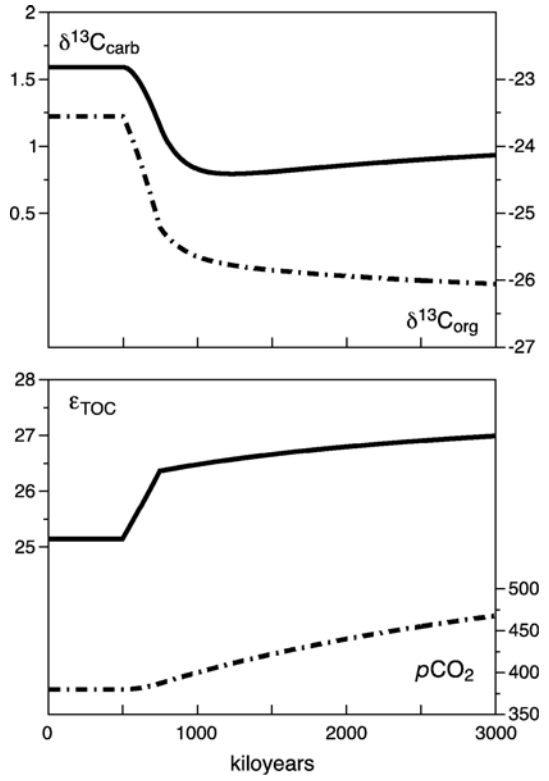

Fig. 5. Results of simulation II. Applied forcing: $[PO_4^{3-}]$ decrease from 0.5 to 0.3 μmol kg^{-1} from timestep 500 to timestep 750.

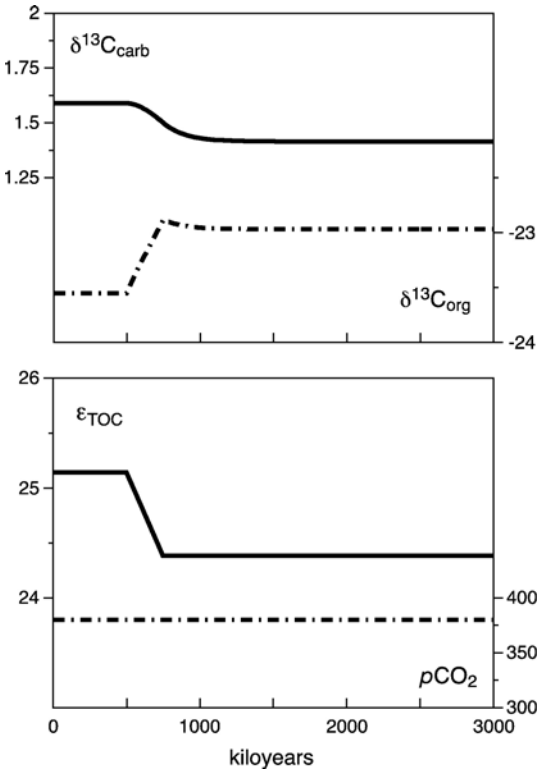

Fig. 6. Results of simulation III. Applied forcing: temperature increase from 15 to 17 °C from timestep 500 to timestep 750.

~1.6‰ for $\delta^{13}C_{carb}$ and −23.5‰ for $\delta^{13}C_{org}$, close to those preceding the interval of rise in ε_{TOC} (Fig. 2).

6. Results of model simulations

6.1. Simulation I: the effect of increasing pCO_2 on ε_{TOC}

Proxy data indicate that during the Late Callovian–Early Oxfordian, pCO_2 levels were considerably lower than before and after [23,33]. Values were possibly as low as 350 ppm in the Late Callovian [23] and around 1000 ppm at the end of the Oxfordian [33]. This apparent rise in pCO_2 might explain the observed increase in ε_{TOC}.

In our model, an increase from pCO_2=380 to 580 ppm within 250 kyr results in a positive shift in $\delta^{13}C_{carb}$ of about 0.5‰, a negative shift in $\delta^{13}C_{org}$ of about 1‰ and thus a 1.5‰ increase in ε_{TOC} (Fig. 4A). Hence, despite

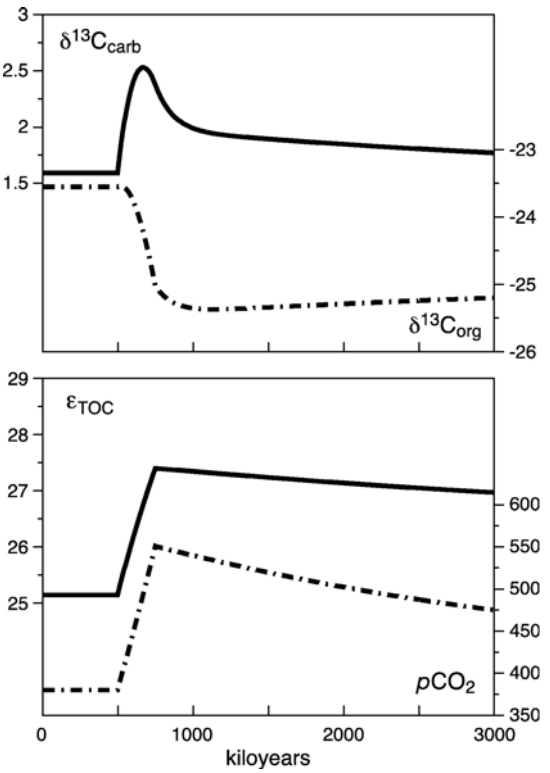

Fig. 7. Results of simulation IV including changes in $F_{d,org}$. Applied forcings: pCO_2 increase from 380 to 570 ppm, $[PO_4^{3-}]$ decrease from 0.5 to 0.35 μmol kg^{-1}, and temperature increase from 15 to 17 °C all from timestep 500 to timestep 750, plus $F_{d,org}$ increase from 6×10^{15} mol kyr^{-1} to 8×10^{15} mol kyr^{-1} at timestep 500.

this rather sharp increase in pCO_2, the model response does not approach the observed values in terms of the amplitude of isotopic change. This is in part because in our model, a higher pCO_2 leads to higher $[PO_4^{3-}]$ as a consequence of the weathering feedback mechanism. Yet increasing $[PO_4^{3-}]$ leads to a smaller ε_{TOC} and thus counteracts the effect of increasing pCO_2 on ε_{TOC}. A doubling of the pCO_2 is necessary to approach the observed increase in ε_{TOC} (Fig. 4B). We consider such an increase unlikely as it could only be achieved by intensive volcanism, methane hydrate dissociation, or oxidation of organic matter, for which (i) geologic evidence is lacking in the Oxfordian [14], and which (ii) would lead to a negative shift in $\delta^{13}C_{carb}$ because of the negative C-isotope compositions of typical mantle- or methane-derived CO_2 and organic matter [10] — a shift that is not observed. Therefore, it is unlikely that an increase in pCO_2 was the only cause of the mid-Oxfordian increase in ε_{TOC}.

6.2. Simulation II: the effect of decreasing [PO43−] on ε_{TOC}

A decrease in $[PO_4^{3-}]$ would lead to a greater ε_{TOC} and thus might explain the isotopic record of the mid-Oxfordian.

In our model, a programmed decrease in $[PO_4^{3-}]$ from 0.5 to 0.3 μmol kg^{-1} within 250 kyr leads to an increase in ε_{TOC} of about 1.5‰, but negative shifts in both $\delta^{13}C_{carb}$ and $\delta^{13}C_{org}$ because the nutrient feedback mechanism in the model reduces the deposition of organic matter (Fig. 5). Therefore, a decrease in $[PO_4^{3-}]$ alone cannot explain the Oxfordian C-isotope record.

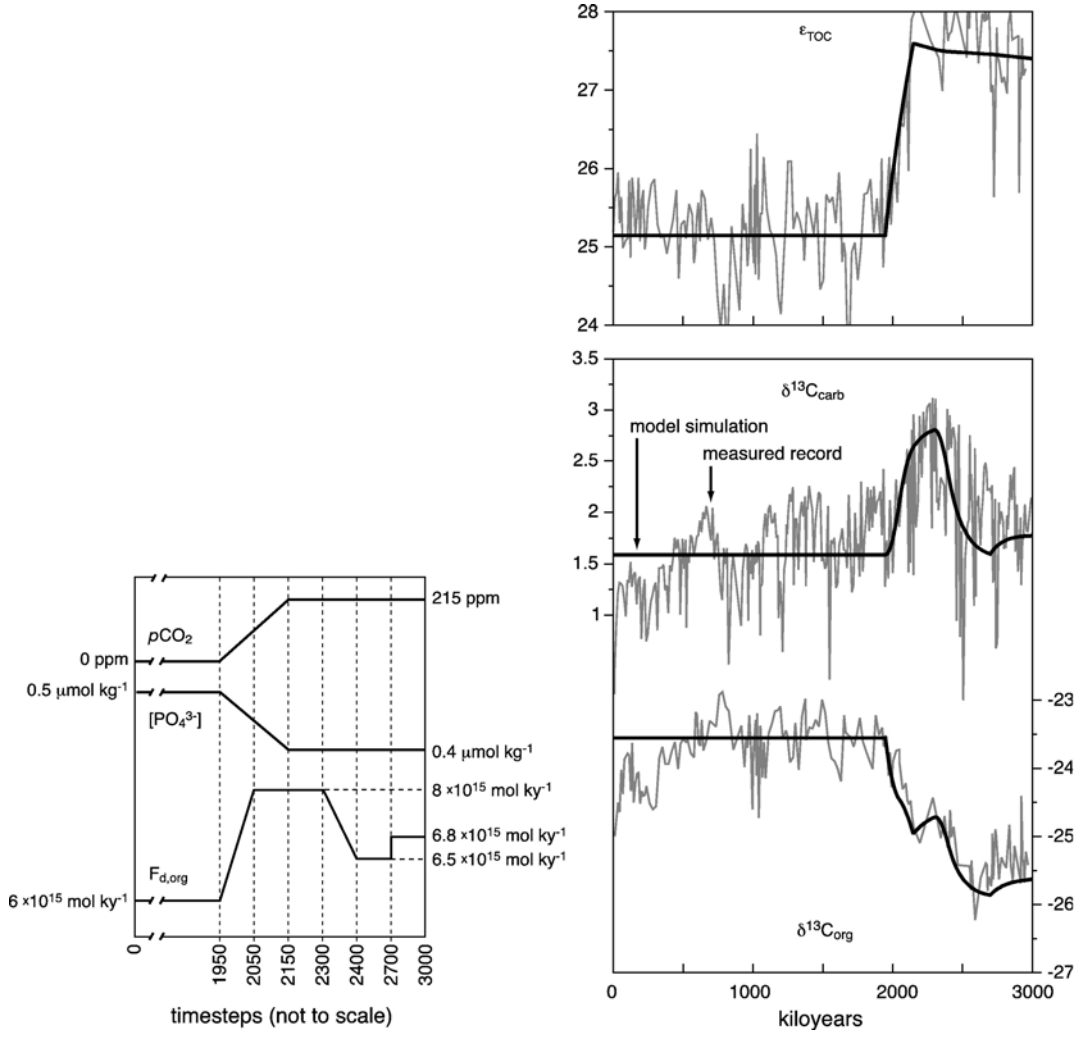

Fig. 8. Forcings to the model applied in simulation V and corresponding results.

6.3. Simulation III: the effect of a temperature increase on ε_{TOC}

Increasing temperature will have the effect of a decrease in ε_{TOC}, because (i) Δ_{carb}, the isotopic difference between CO_2 in water and deposited carbonate, will be smaller [31], and (ii) surface water ability to hold CO_2 in solution is reduced, which will lower ε_P and thus also ε_{TOC}. According to [58], SST increased by less than 2 °C at latitudes between 30 and 40° north, the approximate paleolatitude of the studied section. In our model, a temperature rise of 2 °C within 250 kyr decreases ε_{TOC} by about 0.8‰ (Fig. 6). An increase of 5 °C as indicated by proxy data will have an even more pronounced effect on ε_{TOC}. Therefore, a temperature increase that is not coupled to a rise in pCO_2 or to a decrease in $[PO_4^{3-}]$, cannot explain the Middle Oxfordian isotope record.

6.4. Simulation IV: combining effects of pCO_2, $[PO43-]$ and temperature on ε_{TOC} with increased $F_{d,org}$

In our model, the combined effects of (i) a ~50% increase in pCO_2, (ii) a 30% decrease in $[PO_4^{3-}]$, and a 2 °C increase in SST (all within 250 kyr), produced an increase in ε_{TOC} with a magnitude approaching the observed one. However, although the programmed 30% decrease in $[PO_4^{3-}]$ is attenuated because in the model, higher pCO_2 enhances weathering input of phosphate, $\delta^{13}C_{carb}$ and $\delta^{13}C_{org}$ still experience a negative shift — because deposition of organic matter is reduced through the nutrient feedback mechanism. We find that within reasonable magnitudes of change in the forcing factors, our model is not able to reproduce the observed Middle Oxfordian positive excursion in $\delta^{13}C_{carb}$ solely by changing ε_{TOC}. This may confirm studies proposing that enhanced organic matter deposition ($F_{d,org}$) is the main factor driving positive excursions in $\delta^{13}C_{carb}$ [10,11,59].

In our model, we find that a combination of a 33% higher $F_{d,org}$, a 50% increase in pCO_2, a 30% decrease in $[PO_4^{3-}]$ and a 2 °C increase in temperature reproduces the observed magnitudes of change in ε_{TOC}, $\delta^{13}C_{carb}$ and $\delta^{13}C_{org}$ (Fig. 7).

6.5. Simulation V: reconstructing the measured isotope curves

Here we attempt to simulate as close as possible the measured records of ε_{TOC}, $\delta^{13}C_{carb}$ and $\delta^{13}C_{org}$. The forcing factors applied basically rely on the findings of simulation IV, see Fig. 8. The model response to these forcing factors is very close to the observed Middle Oxfordian isotope record (Fig. 8). There may be other ways to reach a similar output, but not within geologically reasonable values for the forcing factors.

7. Discussion

7.1. Linking the model scenario to Middle Oxfordian geologic data

7.1.1. Increase in pCO_2

One of the key elements in simulation V is a rise in pCO_2 of 215 ppm. There are several possibilities how this could be achieved, including the following:

(i) Intensive volcanism at the scale of large igneous provinces or flood basalts is thought to influence pCO_2 — but there is no geologic evidence for such an event in the Oxfordian [14]. Neither is there evidence for large-scale dissociation of methane hydrate delivering CO_2 to the atmosphere — the negative excursions in the Oxfordian C-isotope record proposed to be related to methane outburst [30] are dated as *transversarium* and *bifurcatus* zone, thus are younger than the proposed increase in pCO_2. Another possibility would be enhanced hydrothermal activity, for which there are indicators in the Middle Oxfordian [15]. However, all of these three mechanisms are expected to create negative shifts in $\delta^{13}C_{carb}$ as they all add ^{13}C-depleted carbon to the ocean–atmosphere reservoir.

(ii) Changes in the amount of carbon stored in terrestrial biomass. This factor is very hard to assess for the Late Jurassic. However, an increase of more than 200 ppm in pCO_2 would require unrealistically large amounts of biomass to be reoxidized (e.g., through wide-spread wildfires). In the present-day situation, the terrestrial biomass would need to be entirely burned to CO_2 to account for a 80 ppm rise in pCO_2 [60]. Furthermore, also this process would add ^{13}C-depleted carbon to the ocean–atmosphere reservoir and likely cause a negative shift in $\delta^{13}C_{carb}$.

(iii) The "coral reef hypothesis" was developed to explain glacial–interglacial changes in pCO_2 of ~80–100 ppm [42,61,62]. The original hypothesis [42] stated that due to rising sea level, conditions became favourable for the expansion of coral reefs, yielding CO_2 through the relationship

$$Ca^{2+} + 2HCO_3^- \rightarrow CaCO_3 + CO_2 + H_2O \qquad (13)$$

A modified "coral reef hypothesis" suggested that, also due to sea-level rise, a shift of the locus of $CaCO_3$

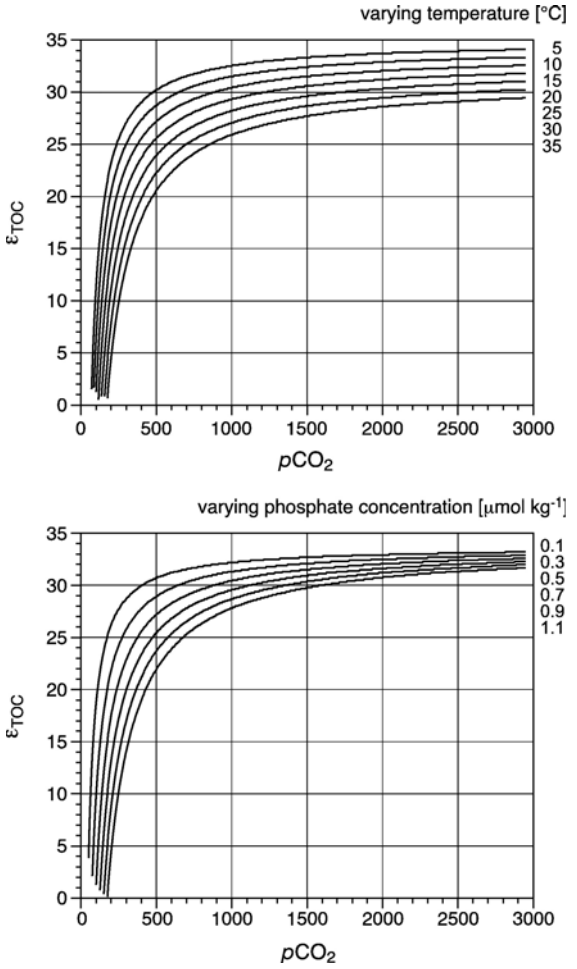

Fig. 9. Response curves for the dependence of ε_{TOC} on pCO_2, $[PO_4^{3-}]$ and temperature. Above: pCO_2 variable at different temperatures and constant $[PO_4^{3-}]=0.5$ µmol kg^{-1}. Below: pCO_2 variable at different $[PO_4^{3-}]$ and constant temperature = 15 °C. ε_{TOC} becomes progressively less sensitive to changes in pCO_2 the higher pCO_2 is.

deposition from deep sea to shallow shelf changed the dissolution–accumulation ratio for $CaCO_3$, which modulated pCO_2 [61]. Thus, also in this case, the increase in pCO_2 is not because of the addition of external CO_2 into the ocean–atmosphere system, but due to a redistribution of carbon between ocean and atmosphere. Both studies agreed in that changes in pCO_2 of as much as 80 ppm are possible by increasing carbonate deposition on shelves (see also [62]). Another version of this hypothesis focused on the shift in the aqueous carbonate equilibrium driven by the removal of carbonate ions in the curse of shallow water carbonate deposition, which increases the partial pressure of CO_2 in the surface ocean [63]. During interglacials, higher levels of pCO_2 are sustained for few hundreds of years to few tens of thousands of years [64]. However, modeling indicates that high pCO_2 may be roughly sustained for several hundreds of thousands of years, basically as long as carbonate deposition predominantly takes places in shallow water regions [65].

Indeed, the Middle Oxfordian has seen one of the most intense spread of shallow water carbonate deposition in earth history [66–68]. In many regions of the western Tethys, platforms became productive again during the upper *plicatilis* zone and flourished during the *transversarium* zone, after an interval of starving in the Late Callovian–Early Oxfordian [22,67]. Thus, the decrease in ε_{TOC} is synchronous to the main expansion phase of reefs and platforms in the Middle Oxfordian. This makes it very likely that the Middle Oxfordian "reef explosion" contributed to the rise in pCO_2 indicated by our data and modeling. Assuming a Middle Oxfordian carbonate deposition area of about 1×10^{12} m^3 on the total shelf area of about 20×10^{12} m^3 [69], and assuming that there, about 40 m of limestone [68] with a porosity of 50% accumulated, we come to a conservative estimate of about 5.4×10^{17} mol carbon deposited during the Middle Oxfordian. The deposition of 10^{17} mol carbon in shallow seas leads to a 40 ppm increase in pCO_2 [63]. Thus, the Middle Oxfordian "reef explosion" may have risen pCO_2 by more than 200 ppm. Shallow-sea carbonate accumulation flourished until the end of the Middle Oxfordian or longer [66,68], giving hand to the idea that higher pCO_2 may have been sustained for several 10^5 yr.

Overall, pCO_2 levels must have been low in the Middle Oxfordian. Steady-state conditions of our model, tuned to represent the situation in the early Middle Oxfordian, ask for a pCO_2 of 380 ppm — a value corroborated by proxy data [23]. Furthermore, at high levels of pCO_2, a change of 3‰ in ε_{TOC} as recorded in our composite section would ask for a magnitude of change in pCO_2 that lies outside reasonable boundaries. Fig. 9 illustrates how ε_{TOC} becomes much less sensitive to changes in pCO_2 at pCO_2 levels above 1000 ppm.

7.1.2. Temperature increase

Modeling indicates that climate in the Middle Oxfordian was influenced by an altered ocean circulation [58]. When the connection between Tethys and Pacific through the Atlantic (Hispanic corridor) became globally significant in terms of water through-flow, it turned on an effective energy exchange from low to high latitudes through ocean currents [58]. Under these conditions, northern high-latitude sea surface temperatures (SST) might increase by 3–11 °C, while tropical SST cool by up to 3 °C [58]. Lithological evidence indicates that this change in ocean circulation took place in the middle of the Oxfordian: marine hardgrounds formed during Middle Callovian to Early Oxfordian are commonly overlain by

regular sediments dated as *plicatilis* to *transversarium* zone, indicating major changes in intermediate-depth currents of the western Tethys at that time [9]. These changes could be due to the opening of the Hispanic corridor [70,71], where we use the term "opening" for the time when water through-flow was high enough to influence the global ocean current system.

The Middle Oxfordian temperature increase at middle latitudes indicated by proxy data [16,18,21,57] may be at least partly the expression of this reorganisation of ocean currents. Northern Tethyan and Boreal basins were influenced by water masses coming from the northern polar latitudes before the opening of the Hispanic corridor, and by much warmer tropical water masses after the opening of the Hispanic corridor [18]. This interpretation is corroborated by the migration of ammonite groups from low to high latitudes within the *plicatilis* zone ([17] and references therein). However, the magnitude of temperature increase predicted by modeling [58] is several degrees below that indicated by proxy data (e.g. [18]). Thus, temperatures probably have been influenced by processes superimposed on ocean circulation changes, as for example an increase in pCO_2 as predicted by our model.

7.1.3. Increased organic carbon burial and decreased phosphate concentration

Organic carbon burial flux ($F_{d,org}$) is difficult to constrain in the Oxfordian. The deposits of the Middle Oxfordian do not feature beds strikingly enriched in organic matter as they occur during Oceanic Anoxic Events (e.g., Toarcian, Valanginian, Aptian). Nevertheless, especially about from the *transversarium* zone onwards, they regionally contain around 1–2% of organic matter [72], an amount already far above that of average pelagic and hemipelagic sediments. Moreover, Oxfordian sediments were identified as major source rocks for some of the world's largest oilfields in the Middle East [73,74]. Therefore, it can be assumed that burial of organic matter was high during parts of the studied interval.

In simulation V, $[PO_4^{3-}]$ slightly decreases, although the programmed 20% decrease is attenuated through the processes described in Section 6.4. This small decrease may be explained with increased productivity, where phosphate would have been consumed and $[PO_4^{3-}]$ would have decreased — a process that could be expected if $F_{d,org}$ was high as discussed above. In summary, input data of simulation V are compatible with available geological data.

We propose the following scenario for the Middle Oxfordian: at the end of the *plicatilis* ammonite zone, changes in the ocean current system resulting from the plate tectonic-induced opening of the Hispanic corridor led to (i) a cooling and drying in low latitudes, warming and drying in middle latitudes, and warming and humidification in high latitudes; (ii) and thus, coupled with sea-level rise, to an explosion-like spread of reefs in low–middle latitudes. Due to the onset of intense carbonate production on shallow shelves, pCO_2 increased. Higher pCO_2, further sea-level rise, and warming triggered enhanced burial of organic matter in shallow epicontinental seas of middle to high latitudes [5]. Enhanced burial of organic matter led to a depletion of nutrients, resulting in the cessation of excess organic matter burial few 10^5 yr after the initiation. The combined effects of rising pCO_2, decreasing nutrient concentrations and a transient enhanced organic matter burial may explain the C-isotope record of the Middle Oxfordian.

7.2. Limitations of the data and the model

The proposed scenario for the Middle Oxfordian matches climate proxy data and lithological evidence. However, the data base for C-isotopes of organic matter is yet very small, and new data may or may not corroborate the record presented here. Further research is needed in order to better constrain timing and impacts of the opening of the Hispanic corridor on the global ocean current system.

The simple model used to develop a scenario for the Middle Oxfordian is limited in various aspects. Especially the feedback mechanisms existing between climate, geosphere and biosphere are far from being completely reproduced in the model. The natural system probably is much more buffered than the model system. Furthermore, alkalinity is assumed to be constant and therefore not treated in the model. Our model results therefore may represent a maximum amplitude of response of the system to forcing, and are highly hypothetical. A more complex model including facilities to simulate spatially resolved carbonate accumulation and its effect on pCO_2 could be employed to test the presented scenario and values, once the geologic data base has become more complete.

8. Conclusions

Based on carbon isotope data and simple model simulations, we propose that the ocean–atmosphere carbon budget and cycle of the Oxfordian were perturbed without any external input of additional carbon. The mid-Oxfordian positive excursion was at least partly caused by an ocean-intrinsic process triggered by plate tectonic movements: when the Tethys–Atlantic–Pacific seaway

became globally significant in terms of water-through-flow, the altered ocean current system diminished latitudinal temperature gradients. Together with sea-level rise promoting the mid-Oxfordian "reef explosion", pCO_2 increased and triggered a response of the carbon cycle that explains the Middle Oxfordian C-isotope record.

Concentration of CO_2 in the atmosphere was possibly as low as 380 ppm in the Early Oxfordian. It may have increased by more than 50% at the end of the *plicatilis* ammonite zone, contributing to and triggering parts of the mid-Oxfordian positive C-isotope excursion. This increase possibly contributed to the Middle Oxfordian temperature increase indicated by proxy data.

The proposed scenario for the Middle Oxfordian is highly hypothetical, but matches available geologic data. Further research with focus on the Oxfordian, a time of major change in carbonate and organic carbon burial will result in an improved geologic data base, needed for the development of more sophisticated models of Late Jurassic carbon cycling.

Acknowledgements

The thoughtful suggestions of two anonymous referees and the editor helped to improve the manuscript. We thank P. Pellenard, P.-Y. Collin and D. Fortwengler for their assistance in the field, and M. Coray for the assistance in the laboratory. Financial support from the Swiss Science Foundation is gratefully acknowledged.

Appendix A. Supplementary data

Supplementary data associated with this article can be found, in the online version, at doi:10.1016/j.epsl.2007.03.014.

References

[1] M. Padden, H. Weissert, H. Funk, S. Schneider, C. Gansner, Late Jurassic lithological evolution and carbon-isotope stratigraphy of the western Tethys, Eclogae Geol. Helv. 95 (2002) 333–346.

[2] B. Louis-Schmid, P. Rais, S.M. Bernasconi, P. Pellenard, P.-Y. Collin, H. Weissert, Detailed record of the mid-Oxfordian (Late Jurassic) positive carbon-isotope excursion in two hemipelagic records (France and Switzerland): a plate tectonic trigger? Palaeogeogr. Palaeoclimatol. Palaeoecol. (in press), doi:10.1016/j.palaeo.2007.01.001.

[3] C.R. Pearce, S.P. Hesselbo, A.L. Coe, The mid-Oxfordian (Late Jurassic) positive carbon-isotope excursion recognised from fossil wood in the British Isles, Palaeogeogr. Palaeoclimatol. Palaeoecol. 221 (2005) 343–357.

[4] A. Maheshwari, A.N. Sial, S.C. Mathur, R.P. Tripathi, $\delta^{13}C$ Variations in Late Jurassic Carbonates, Jaisalmer Formation, Western India, Gondwana Res. 6 (2003) 931–934.

[5] H.C. Jenkyns, Relative sea-level change and carbon isotopes: data from the Upper Jurassic (Oxfordian) of central and Southern Europe, Terra Nova 8 (1996) 75–85.

[6] H. Wierzbowski, Detailed oxygen and carbon isotope stratigraphy of the Oxfordian in Central Poland, Int. J. Earth Sci. (Geol. Rundsch.) 91 (2002) 304–314.

[7] V. Lavastre, Evènements sédimentaires, diagénétiques et post-diagénétiques dans la formation argileuse du Callovo-Oxfordien (Bassin de Paris, France): enregistrement isotopique des minéraux et de l'eau porale, PhD, Université Paris VII, 2002.

[8] M.E. Katz, J.D. Wright, K.G. Miller, B.S. Cramer, K. Fennel, P.G. Falkowski, Biological overprint of the geological carbon cycle, Mar. Geol. 217 (2005) 323–338.

[9] P. Rais, B. Louis, S. Bernasconi, H. Weissert, Evidence for changes in intermediate-water currents in the Alpine Tethys during the Late Jurassic, Geophys. Res. Abstr. 7 (2005) 06583.

[10] L.R. Kump, M.A. Arthur, Interpreting carbon-isotope excursions: carbonates and organic matter, Chem. Geol. 161 (1999) 181–198.

[11] M.A. Arthur, W.E. Dean, S.O. Schlanger, Variations in the global carbon cycle during the Cretaceous related to climate, volcanism, and changes in atmospheric CO_2, in: E.T. Sundquist, W.S. Broecker (Eds.), The Carbon Cycle and Atmospheric CO_2: Natural Variations Archean to Present, Geophysical Monograph, vol. 32, American Geophysical Union, Washington, DC, 1985, pp. 504–529.

[12] R.L. Larson, E. Erba, Onset of the mid-Cretaceous greenhouse in the Barremian–Aptian: igneous events and the biological, sedimentary, and geochemical responses, Paleoceanography 14 (1999) 663–678.

[13] H. Weissert, E. Erba, Volcanism, CO_2 and palaeoclimate: a Late Jurassic–Early Cretaceous carbon and oxygen isotope record, J. Geol. Soc. (Lond.) 161 (2004) 695–702.

[14] C.E. Jones, H.C. Jenkyns, Seawater strontium isotopes, oceanic anoxic events, and seafloor hydrothermal activity in the Jurassic and Cretaceous, Am. J. Sci. 301 (2001) 112–149.

[15] J.-P. Cogné, E. Humler, Temporal variation of oceanic spreading rate and crustal production rates during the last 180 My, Earth Planet. Sci. Lett. 227 (2004) 427–439.

[16] O. Abbink, J. Targarona, H. Brinkhuis, H. Visscher, Late Jurassic to earliest Cretaceous paleoclimatic evolution of the southern North Sea, Glob. Planet. Change 30 (2001) 231–256.

[17] G. Dromart, J.P. Garcia, S. Picard, F. Atrops, C. Lécuyer, S.M.F. Sheppard, Ice age at the Middle–Late Jurassic transition? Earth Planet. Sci. Lett. 213 (2003) 205–220.

[18] A. Riboulleau, F. Baudin, V. Daux, P. Hantzpergue, M. Renard, V. Zakharov, Évolution de la paléotempérature des eaux de la plate-forme russe au cours du Jurassique supérieur (Sea surface paleotemperature evolution of the Russian Platform during the Upper Jurassic), C.R. Acad. Sci. Paris, Sciences de la terre et des planètes 326 (1998) 239–246.

[19] B.G.K. van Aarssen, R. Alexander, R.I. Kagi, Higher plant biomarkers reflect palaeovegetation changes during Jurassic times, Geochim. Cosmochim. Acta 64 (2000) 1417–1424.

[20] V.A. Vakhrameyev, Classopollis pollen as an indicator of Jurassic and Cretaceous climate, Int. Geol. Rev. 24 (1982) 1190–1196.

[21] Y. Hautevelle, R. Michels, F. Malartre, A. Trouiller, Vascular plant biomarkers as proxies for palaeoflora and palaeoclimatic changes at the Dogger/Malm transition of the Paris Basin (France), Org. Geochem. 37 (2006) 610–625.

[22] F. Cecca, B. Martin Garin, D. Marchand, B. Lathuiliere, A. Bartolini, Paleoclimatic control of biogeographic and sedimentary events in

Tethyan and peri-Tethyan areas during the Oxfordian (Late Jurassic), Palaeogeogr. Palaeoclimatol. Palaeoecol. 222 (2005) 10–32.
[23] C.J. Yapp, H. Poths, Carbon isotopes in continental weathering environments and variations in ancient atmospheric CO_2 pressure, Earth Planet. Sci. Lett. 137 (1996) 71–82.
[24] N.-P. Tribovillard, Géochimie organique et minérale dans les Terres Noires calloviennes et oxfordiennes du abssin dauphinois (France SE): mise en évidence de cycles climatiques, Bull. Soc. Géol. Fr. 8 (1988) 141–150.
[25] E.E. Bray, E.D. Evans, Distribution of n-paraffins as a clue to recognition of source beds, Geochim. Cosmochim. Acta 22 (1961) 2–15.
[26] W.K. Seifert, J.M. Moldowan, The effect of thermal stress on source-rock quality as measured by hopane stereochemistry, in: A.G. Douglas, J.R. Maxwell (Eds.), Advances in Organic Geochemistry, Pergamon Press, Oxford, 1979, pp. 229–237.
[27] H.L. ten Haven, J.W. de Leeuw, J. Rullkötter, J.S. Sinninghe Damsté, Restricted utility of the pristane/phytane ratio as a palaeoenvironmental indicator, Nature 330 (1987) 641–643.
[28] K.E. Peters, J.M. Moldowan, The Biomarker Guide: Interpreting Molecular Fossils in Petroleum and Ancient Sediments, Prentice-Hall, 1993 363 pp.
[29] P.A. Meyers, Preservation of elemental and isotopic source identification of sedimentary organic matter, Chem. Geol. 114 (1994) 289–302.
[30] M. Padden, H. Weissert, M. de Rafelis, Evidence for Late Jurassic release of methane from gas hydrate, Geology 29 (2001) 223–226.
[31] J.M. Hayes, H. Strauss, A.J. Kaufman, The abundance of ^{13}C in marine organic matter and isotopic fractionation in the global biogeochemical cycle of carbon during the past 800 Ma, Chem. Geol. 161 (1999) 103–125.
[32] M. Pagani, The alkenone-CO_2 proxy and ancient atmospheric carbon dioxide, Philos. Trans. R. Soc. Lond., A 360 (2002) 609–632.
[33] K.H. Freeman, J.M. Hayes, Fractionation of carbon isotopes by phytoplankton and estimates of ancient CO_2 levels, Glob. Biogeochem. Cycles 6 (1992) 185–198.
[34] J.M. Hayes, Factors controlling ^{13}C contents of sedimentary organic compounds: principles and evidence, Mar. Geol. 113 (1993) 111–125.
[35] M.D. Lewan, Effects of thermal maturation on stable organic carbon isotopes as determined by hydrous pyrolysis of Woodford Shale, Geochim. Cosmochim. Acta 47 (1983) 1471–1479.
[36] R.R. Bidigare, A. Fluegge, K.H. Freeman, K.L. Hanson, J.M. Hayes, D. Hollander, J.P. Jasper, L.L. King, E.A. Laws, J. Milder, F.J. Millero, R. Pancost, B.N. Popp, P.A. Steinberg, S.G. Wakeham, Consistent fractionation of ^{13}C in nature and in the laboratory: growth-rate effects in some haptophyte algae, Glob. Biogeochem. Cycles 11 (1997) 279–292.
[37] L. Wissler, Response of Early Cretaceous sedimentary systems to perturbations in global carbon cycling: insights from stratigraphy, sedimentology and geochemical modeling, Diss. ETH Nr. 14380 PhD, ETH Z. ürich, 2001.
[38] C.R. Romanek, E.L. Grossman, J.W. Morse, Carbon isotopic fractionation in synthetic aragonite and calcite: effects of temperature and precipitation rate, Geochim. Cosmochim. Acta 56 (1992) 419–430.
[39] R.F. Weiss, Carbon dioxide in water and seawater: the solubility of a non-ideal gas, Mar. Chem. 2 (1974) 203–215.
[40] R.E. Zeebe, D. Wolf-Gladrow, CO_2 in Seawater: Equilibrium, Kinetics, Isotopes, Elsevier, 2001.
[41] J.C. Zachos, L.R. Kump, Carbon cycle feedbacks and the initiation of Antarctic glaciation in the earliest Oligocene, Glob. Planet. Change 47 (2005) 51–66.
[42] W.H. Berger, Increase of carbon dioxide in the atmosphere during deglaciation: the coral reef hypothesis, Naturwissenschaften 69 (1982) 87–88.
[43] J.R. Toggweiler, J.L. Russell, S.R. Carson, Midlatitude westerlies, atmospheric CO_2, and climate change during the ice ages, Paleoceanography 21 (2006) PA2005.
[44] R. Revelle, H.E. Suess, Carbon dioxide exchange between atmosphere and ocean and the question of an increase of atmospheric CO_2 during the past decades, Tellus 9 (1957) 18–27.
[45] D.J. Beerling, R.A. Berner, Feedbacks and the coevolution of plants and atmospheric CO_2, Proc. Natl. Acad. Sci. 102 (2005) 1302–1305.
[46] R.A. Berner, K. Caldeira, The need for mass balance and feedback in the geochemical carbon cycle, Geology 25 (1997) 955–956.
[47] A. Ridgwell, R.E. Zeebe, The role of the global carbonate cycle in the regulation and evolution of the Earth system, Earth Planet. Sci. Lett. 234 (2005) 299–315.
[48] K. Wallmann, Controls on the Cretaceous and Cenozoic evolution of seawater composition, atmospheric CO_2 and climate, Geochim. Cosmochim. Acta 65 (2001) 3005–3025.
[49] T. Tyrrell, The relative influences of nitrogen and phosphorus on oceanic primary production, Nature 400 (1999) 525–531.
[50] D.E. Canfield, Factors influencing organic carbon preservation in marine sediments, Chem. Geol. 114 (1994) 315–329.
[51] K.B. Föllmi, 160 m.y. record of marine sedimentary phosphorus burial: coupling of climate and continental weathering under greenhouse and icehouse conditions, Geology 23 (1995) 859–862.
[52] P.N. Froelich, M.L. Bender, N.A. Luedtke, G.R. Heath, T. DeVries, The marine phosphorus cycle, Am. J. Sci. 282 (1982) 474–511.
[53] P. Van Cappellen, E.D. Ingall, Redox stabilization of the atmosphere and oceans by phosphorus-limited marine productivity, Science 271 (1996) 493–496.
[54] K. Wallmann, Feedbacks between ocaenic redox states and marine productivity: a model perspective focused on benthic phosphorus cycling, Glob. Biogeochem. Cycles 17 (2003) 1084.
[55] L.M. François, Y. Godderis, Isotopic constraints on the Cenozoic evolution of the carbon cycle, Chem. Geol. 145 (1998) 177–212.
[56] Hay W.W., A. Migdisov, A.N. Balukhovsky, C.N. Wold, S. Flogel, E. Soding, Evaporites and the salinity of the ocean during the Phanerozoic: implications for climate, ocean circulation and life, Palaeogeogr. Palaeoclimatol. Palaeoecol. 240 (2006) 3–46.
[57] C. Lécuyer, S. Picard, J.-P. Garcia, S.M.F. Sheppard, P. Grandjean, G. Dromart, Thermal evolution of Tethyan surface waters during the Middle–Late Jurassic: evidence from $\delta^{18}O$ values of marine fish teeth, Paleoceanography 18 (2003) 1076.
[58] R.M. Hotinski, J.R. Toggweiler, Impact of a Tethyan circumglobal passage on ocean heat transport and "equable" climates, Paleoceanography 18 (2003) 1007.
[59] H. Weissert, A. Lini, K.B. Föllmi, O. Kuhn, Correlation of Early Cretaceous carbon isotope stratigraphy and platform drowning events: a possible link? Palaeogeogr. Palaeoclimatol. Palaeoecol. 137 (1998) 189–203.
[60] D. Archer, A. Winguth, D. Lea, N. Mahowald, What caused the glacial/interglacial atmospheric pCO_2 cycles? Rev. Geophys. 38 (2000) 159–189.
[61] B.N. Opdyke, J.C.G. Walker, Return of the coral reef hypothesis: basin to shelf partitioning of $CaCO_3$ and its effect on atmospheric CO_2, Geology 20 (1992) 733–736.
[62] A. Vecsei, W.H. Berger, Increase of atmospheric CO_2 during deglaciation: constraints on the coral reef hypothesis from patterns of deposition, Glob. Biogeochem. Cycles 18 (2004) GB1035.

[63] A.J. Ridgwell, A.J. Watson, M.A. Maslin, J.O. Kaplan, Implications of coral reef buildup for the controls on atmospheric CO_2 since the Last Glacial Maximum, Paleoceanography 18 (2003) 1083.

[64] J.R. Petit, J. Jouzel, D. Raynaud, N.I. Barkov, J.M. Barnola, I. Basile, M. Bender, J. Chappellaz, M. Davis, G. Delaygue, M. Delmotte, V.M. Kotlyakov, M. Legrand, V.Y. Lipenkov, C. Lorius, L. Pepin, C. Ritz, E. Saltzman, M. Stievenard, Climate and atmospheric history of the past 420,000 years from the Vostok ice core, Antarctica, Nature 399 (1999) 429–436.

[65] A.J. Ridgwell, M.J. Kennedy, K. Caldeira, Carbonate deposition, climate stability, and Neoproterozoic ice ages, Science 302 (2003) 859–862.

[66] R.R. Leinfelder, D.U. Schmid, M. Nose, W. Werner, Jurassic reef patterns; the expression of a changing globe, in: W. Kiessling, E. Flügel, J. Golonka (Eds.), Phanerozoic Reef Patterns, Special Publication — Society for Sedimentary Geology, vol. 72, 2002, pp. 465–520.

[67] E. Insalaco, Upper Jurassic microsolenid biostromes of northern and central Europe: facies and depositional environment, Palaeogeogr. Palaeoclimatol. Palaeoecol. 121 (1996) 169–194.

[68] G. Dromart, J.-P. Garcia, F. Gaumet, S. Picard, M. Rousseau, F. Atrops, C. Lecuyer, S.M.F. Sheppard, Perturbation of the carbon cycle at the Middle/Late Jurassic transition: geological and geochemical evidence, Am. J. Sci. 303 (2003) 667–707.

[69] L.J. Walker, B.H. Wilkinson, L.C. Ivany, Continental drift and phanerozoic carbonate accumulation in shallow-shelf and deep-marine settings, J. Geol. 110 (2002) 75–87.

[70] M. Meschede, W. Frisch, A plate-tectonic model for the Mesozoic and Early Cenozoic history of the Caribbean plate, Tectonophysics 296 (1998) 269–291.

[71] A.C. Riccardi, Jurassic and Cretaceous marine connections between the Southeast Pacific and Tethys, Palaeogeogr. Palaeoclimatol. Palaeoecol. 87 (1991) 155–189.

[72] H.C. Jenkyns, C.E. Jones, D.R. Gröcke, S.P. Hesselbo, D.N. Parkinson, Chemostratigraphy of the Jurassic System: applications, limitations and implications for paleoceanography, J. Geol. Soc. (Lond.) 159 (2002) 351–378.

[73] AS. Alsharan, G.L. Wittle, Carbonate-evaporite sequences of the Late Jurassic, Southern and Southwestern Arabian Gulf, AAPG Bull. 79 (1995) 1608–1630.

[74] R.J. Murris, Middle East: stratigraphic evolution and oil habitat, AAPG Bull. 64 (1980) 597–618.

[75] A.G. Smith, D.G. Smith, B.M. Funnell, Atlas of Mesozoic and Cenozoic Coastlines, Cambridge Univ. Press, Cambridge, 1994 99 pp.

[76] P.A. Ziegler, Evolution of the Arctic–North Atlantic and the Western Tethys, AAPG Mem. 43 (1988) 198.

[77] U.G. Wortmann, H. Weissert, H. Funk, J. Hauck, Alpine plate kinematics revisited: the Adria Problem, Tectonics 20 (2001) 134–147.